ORIGINAL ARTICLE

Poly(vinyl alcohol)/poly(glycerol) dendrimer hydrogel mediated green synthesis of silver nanoparticles

Pollyana Marcondes[1] , Gisela Helou Rosas[2] , Maria Elena Leyva González[1*] ,
Alvaro Antonio Alencar de Queiroz[3] and Paulo Sergio Marques[4]

¹*Instituto de Físico Química, Universidade Federal de Itajubá, Itajubá, MG, Brasil*
²*Faculdade Wenceslau Braz, Itajubá, MG, Brasil*
³*Centro de Biotecnologia, Instituto de Pesquisas Energéticas e Nucleares, São Paulo, SP, Brasil*
⁴*Laboratório de Microbiologia Aplicada, Instituto de Recursos Naturais, Universidade Federal de Itajubá, Itajubá, MG, Brasil*
*mariae@unifei.edu.br

Abstract

In this paper, we report the synthesis and evaluation of a poly(vinyl alcohol)/poly(glycerol) dendrimer hydrogel incorporated with green synthesized silver nanoparticles (PVA/PGLD-AgNPs) using Cinnamomum verum extract as the reducing agent (Cz-extract). The Cz-extract was prepared using ultrasonic technique. UV-visible (UV-vis) spectra of Cz-extract confirmed the presence of cinnamaldehyde. PVA/PGLD-AgNPs films were prepared using 5, 10 and 20 mL of Cz-extract and characterized by UV-vis, Fourier transform infrared spectroscopy, Thermogravimetric analysis and X-ray diffraction (XRD). The surface plasmon resonance band in the UV-vis spectra confirmed the formation of AgNPs. XRD pattern confirmed the presence of silver, with average crystallite sizes calculated by Scherrer equal to 13.64 nm, 16.63nm and 20.27 nm for AgNPs prepared with 5 mL, 10 mL and 20 mL of Cz-extract, respectively. AgNPs release kinetic was studied by Korsmeyer– Peppas model. The antimicrobial results revealed that the PVA/PGLD-AgNPs hydrogels showed good antibacterial activity behavior against Escherichia coli.

Keywords: *Cinnamomum verum bark, green synthesis, poly(glycerol) dendrimer, poly(vinyl alcohol), silver nanoparticles.*

1. Introduction

Burn wounds are one of the most common household injuries[1]. Burns represent the fourth most common type of trauma worldwide[2] and the second leading cause of hospitalizations in Brazil[3]. Unfortunately, in Brazil, as in other countries, the social isolation promoted by the COVID-19 pandemic has hit the low-income population hard. Although the price of cooking gas in the country has increased by almost 30% in the 12 months to March 2022, 56% of the Brazilian population has seen their income drop since the beginning of the pandemic. With the worsening of the economic and social crisis, families in need have been pressured to use alternative, more flammable and dangerous fuels to prepare their meals. The result is that domestic accidents with severe burns have now become more common in Brazil[4,5].

For centuries, metal, ions and silver compounds have extensively been used for hygienic and healing purposes, due to their strong bactericidal effects and antimicrobial properties[6]. In the 19th century, silver in the form of silver salts or silver solutions began to be used as dressing wounds in burns injuries[7]. Silver sulfadiazine was introduced

by Fox in the 1970s for topical treatment of burns and wounds and remains to this day as the most widely used substances[8]. In the last decade of the 20th century there has been a great innovation in wound care products based on silver nanoparticles. These products are nowadays based on silver in the form of nanocrystalline, ions or compounds incorporated within the dressing[9,10].

The use of silver nanoparticles (AgNPs) for treatment of burns is considered a multi-target process[11]. In addition of AgNPs attaching to the cell membranes and damaging the integrity and permeability of the membranes, they can produce reactive oxygen species (ROS). The ROS act damaging the cell membranes and react with the molecules in the functional proteins and DNA, which will interfere with the metabolism and DNA duplication of microorganisms[12-14].

Several methods have been used to prepare metal nanoparticles[15]. Besides physical and chemical methods, generally hazardous to the environment and very expensive, green synthesis methods result in a simple and ecologically appropriate way to obtain nanoparticles[16]. Green synthesis,

also known as phyto-synthesis, consists of the use of phytochemical compounds, with reducing properties and capping agent to stabilize the synthesized nanoparticles. The phyto-synthesis of nanoparticles can be either, intracellular or extracellular. The intracellular method consists in the synthesis of nanoparticles during the process of growth of the plant, in an organic medium containing metal ions. However, the extracellular method is more simple and consists of the use of some appropriate vegetal extract[17].

The extracellular phyto-synthesis method has several advantages to obtain metal nanoparticles, firstly, the plants are easily accessible, safe to handle, and have a great variety of phytochemical compounds. In the second place, many plants are well known by their medicinal properties, that could enhance the therapeutic efficiency of the nanoparticle[18].

The *Cinnamomum verum* is a medicinal plant with well known therapeutic properties, such as anti-oxidant, anti-diabetic, antimicrobial and anti-inflammatory effects[18-23]. Several authors have used different parts of *Cinnamomum verum* plants to perform green synthesis of nanoparticles[18,24-27].

In this work, the vegetal extract of *Cinnamomum verum* back powder was assisted by ultrasound technique and characterized by UV-visible spectroscopy (UV-vis), Fourier transform infrared spectroscopy (FTIR) and Thermogravimetric analysis (TGA). The aqueous extract of *Cinnamomum verum* (Cz-extract) was used for the green synthesis of silver nanoparticles (AgNPs) mediated by poly(vinyl alcohol)/poly(glycerol) dendrimer (PVA/PGLD) hydrogel blends as reducing and capping agents, respectively. Hydrogel films of PVA/PGLD-AgNPs were prepared using 5, 10, and 20 mL of Cz-extract and characterized by UV-vis, FTIR, TGA and X-ray diffraction (XDR) techniques. The AgNPs release studies from hydrogels were realized for all PVA/PGLD-AgNPs formulations at room temperature (25 °C). The kinetics of AgNPs release from PVA/PGLD-AgNPs hydrogels were studied by Higuchi and Korsmeyer–Peppas model. Finally, the antibacterial properties of PVA/PGLD-AgNPs hydrogels were tested against *Escherichia coli (E.coli)* using the agar disk diffusion method.

2. Materials and Methods

2.1 Materials

Poly(vinyl alcohol) (PVA) 87-90% hydrolyzed with average molecular weight of 30-70 kDa and silver nitrate (99,0%) purity were purchased from Sigma-Aldrich (Brazil). Poly(glycerol) dendrimer of generation 4 was synthesized in accordance with previous work[28]. *Cinnamomum verum* bark powder was acquired from local commerce was washed with distilled water to remove eventual impurities and allowed to dry for 24 h at 60°C.

2.2 Green synthesis of silver nanoparticles in PVA/PGLD hydrogels

The aqueous extract of *Cinnamomum verum* bark powder was prepared by ultrasound assisted extraction. For each 1g of powder it was added 50 mL of distilled water and the aqueous powder suspension was kept in an ultrasonic bath (40 kHz) at 50°C for 60 min. The supernatant was filtered

through a 0.2 μm filter followed by lyophilization to obtain the Cz-extract.

The PVA hydrogels preparation was carried out by mixing a 0.8 g of PVA powder in 20 mL of distilled water under constant stirring at room temperature (25 °C) over a period of 24h until a homogeneous solution was obtained. Then, while constantly stirring, 2.0 g of PGLD was added. Later, the final solution of the PVA-PGLD pre-gel was transferred to three Erlenmeyer flasks. Subsequently, the PVA-PGLD pre-gel and Cz-extract solutions were mixed to obtain the final PVA-PGLD/Cz-extract proportions (v/v) of 95:5 (film PVA-PGLD5), 90:10 (film PVA-PGLD10) and 80:20 (film PVA-PGLD20). Finally, silver nitrate aqueous solution at concentration of 3.7 mM was added to each Erlenmeyr flask under constant stirring (300 rpm) for 24 h avoiding as much as possible light contact, until a homogeneous PVA-PGLD solution was obtained. Afterwards, 25 mL of each mixture was casted into polytetrafluoroethylene (PTFE) plates (100 cm²) and left to dry at 35 °C and controlled relative humidity (64%) for 168 h. Finally, the resulting films were washed with deionized water and dried at 37 °C before use.

2.3 Physico-chemical characterization

2.3.1 UV-Vis, ATR-FTIR and TGA analysis

The Cz-extract and prepared PVA/PGLD-AgNPs hydrogels were characterized by UV-Vis, ATR-FTIR and TGA, respectively. A Cary 50 Varian UV-Vis spectrometer was used in the characterization of Cz-extracts and AgNPs. The UV-Vis experiments were carried out in quartz cells using deionized water as solvent and the spectra were collected from 250 to 500 nm. The deconvolution of UV–vis spectra was realized with the software Origin®.

All samples were analyzed through FTIR Shimadzu IRTracer 100 spectrometer provided by an ATR diamond accessory. The spectrum was obtained on transmittance mode and was scanned registering the spectrum with 30 scans at a resolution of 4 cm^{-1}, from 4000 to 650 cm^{-1}.

TGA measurements were carried out using a TGA-60, Shimadzu, Japan at a constant heating rate of 20 °C min^{-1} from 25 to 800 °C under nitrogen atmosphere (50 mL.min^{-1}).

Powder X-ray diffractograms were collected at room temperature (25°C) using a X'Pert PRO, Malvern Panalytical, Cu Kα radiation (λ = 1.5417 Å) source, operating at 40 kV and 40 mA. Powder diffractograms were collected over an angular 2θ range between 5° and 90° (2θ) with a step size of 0.02° and scanning speed of 2 sec/step.

2.3.2 Release profile of AgNPs from the hydrogels

The release of AgNPs from the PVA/PGLD-AgNPs films was studied in deionized water at room temperature (25°C). The PVA/PGLD-AgNPs films were immersed in deionized water (5 mL) at test tubes and put in thermal bath at 25°C without agitation. The films were carefully adhered to the test tube walls to ensure that they could be entirely submersed. At specific time intervals, the test tube was removed from the thermal bath and the absorbance measurements were at 440 nm and room temperature (25°C) using UV-Vis.

To study the release kinetics of AgNPs, the Korsmeyer-Peppas[29] and Higuchi[30] kinetics models were used.

The Korsmeyer-Peppas model (Equation 1) is a combination of the diffusion of the AgNPs (Fickian transport) from the PVA-PGLD hydrogels and Case II transport (non-Fickian) [29]. In the Higuchi's model[30] (Equation 2), the erosion of the hydrogel matrix as well as its intumescence control the release rate of the nanoparticles, resulting in a AgNPs layer on the PVA-PGLD hydrogel surface and thus, prevent the entry of more water and prevent the release of more nanoparticles, resulting in decline of the AgNPs concentration over time. The diffusion models of Korsmeyer-Peppas and Higuchi are presented below:

$$\frac{M_t}{M_\infty} = k_{KP} * t^n \qquad (1)$$

$$Q_t = K_H * t^{0.5} \qquad (2)$$

where M_t/M_∞ is the fraction of AgNPs released at time t, k_{KP} is the kinetic rate constant for Korsmeyer-Peppas model, and n is the release exponent characterizing the different release mechanisms, k_H is the release rate constant for the Higuchi model and Q_t is the amount of the active principle released in time t.

2.4 Antibacterial activity

The in vitro antibacterial activity of PVA/PGLD-AgNPs system were tested against *Escherichia coli (E.coli)* by agar disk-diffusion method[31]. The *E. coli* bacteria were grown in nutrient broth to prepare stock solutions of 100 µg/mL. Firstly, the filter paper disc (6 mm in diameter) was sterilized in a laminar air flow chamber by exposure to a UV-C lamp (30 min, distance from the lamp 60 cm). A soft-top agar (1.0 wt %, 20 mL) was melted, cooled to 55 °C and inoculated with overnight (18 h) bacteria cultures (200 µL), then gently stirred and poured over previously solidified nutrient agar base in sterile Petri dishes. The number of bacteria in the nutrient soft-top agar layer was set to be 1.5×10^8 CFU. mL^{-1}. After solidification of soft-top agar diffusion discs, 10 µL samples of PVA/PGLD-AgNPs reaction solution were placed on their surface. The widths of inhibition zones around the disk were measured after incubation at 37 °C for 24 h. Each essay was carried out in triplicate.

3. Results and Discussions

3.1 Characterization of Cinnamomum verum aqueous extract

The UV–vis spectra of *Cinnamomum verum* aqueous extract (Cz-extract) and its deconvolution are shown in Figure 1. Two absorption bands centered at ~281 nm and ~300 nm were observed. The band centered at 281 nm can be assigned to n→π* electronic transitions of the carbonyl groups of Cinnamaldehyde[32,33].

The ultrasound assisted extraction is more effective and can increase the number of secondary metabolites extracted from vegetal matrices[34]. Hence, the absorbance band next to 300 nm can be linked to n→π* transitions of phenol, flavonoids or other secondary metabolites present in *Cinnamomum verum* bark[19].

The FTIR spectrum of lyophilized Cz-extract (Figure 2) was performed to identify the functional groups of the active components presents in the aqueous extract. The vibrational band next to 3282 cm⁻¹ is due to the O-H stretching of alcohols and phenols groups. The band at 2927 cm⁻¹ revealed the presence of -CH₂ stretch. The 1649 cm⁻¹ and 1606 cm⁻¹ bands were linked to C=O and -C=C – stretchings, respectively[27], and the 1439 cm⁻¹ band is due to C-H bending. The vibrational band at 1035 cm⁻¹ indicates the C-O-C stretching, therefore suggesting the presence of glycosides group[20].

The Thermogravimetric analysis (TGA) and their differential thermal (DTG) analysis were examined to determine the thermochemical behavior of the lyophilized Cz-extract. The curves of TGA and DTG for Cz-extract are shown in Figure 3. The DTG curve suggests that thermal degradation of the Cz-extract occurs in four stages. The very first decomposition (7% of weight loss) was in the temperature level of 25 °C to 115 °C and was for the removal of moisture available in the sample. Stage 2 (9% weight loss) was recorded up to 115 to 220 °C for the sample, showing the elimination of volatile essential oils available in the sample. Stage 3 (19% of weight loss) recorded between 220 to 330°C, may be due to the thermal decomposition of carbohydrates and proteins. The percentage of weight loss in this stage was comparable with the results
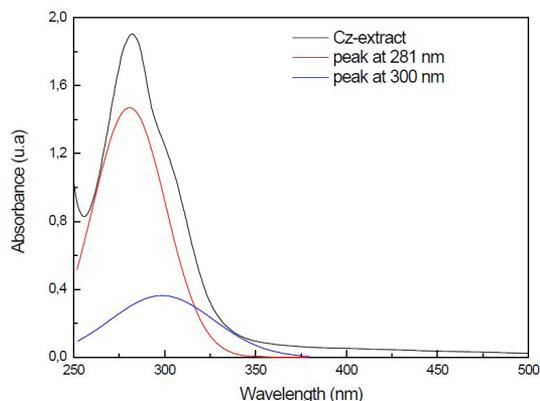

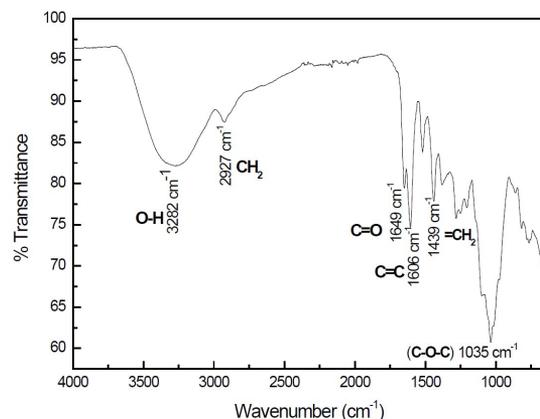**Figure 1.** UV–vis from *Cinnamomum verum* aqueous extract.

Figure 2. FTIR spectrum of lyophilized Cz-extract.

of literature[35]. Stage 4 was recorded up to 330 to 600 °C for the Cz-extract sample, showing the elimination of extractable macromolecules wich high thermal stability. The main decomposition which occurred in this stage is 50% of weight loss for the breakdown of the extractable macromolecules, probably the presence of lipids due to the strong extraction procedures employed. The residual mass was found to be around 15% after 600 °C temperature.

3.2 Physico-chemical characterization of PVA/PGLD-AgNPs films.

The chemical groups present in the Cz-extract, such as aldehyde and alcohols, can reduce the silver ions into nanocrystals. The silver nanoparticles formed by chemical reduction are stabilized by the biological macromolecules
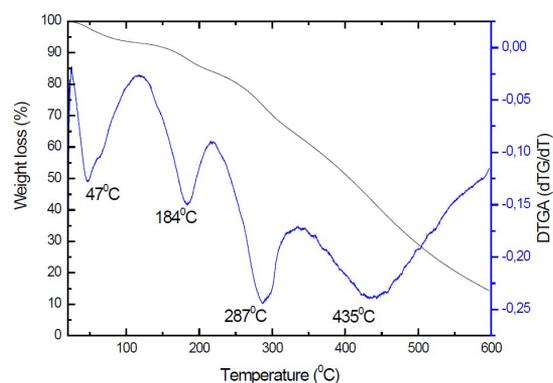
and the polymeric system used. Figure 4 shows the scheme of green synthesis of AgNPs due to the presence of Cinnamaldehyde in the Cz-extract. The AgNPs are sterically stabilized largely by PVA and PGLD, polymeric system. Also in the same Figure 4 is shown the hydrogel PVA/PGLD-AgNPs10 obtained after casting on PTFE plates.

UV-Vis spectroscopy is an indirect method to examine the formation of AgNPs in PVA/PGLD hydrogels, through the absorption band relative to the surface plasmon resonance (SPR)[36].

Figure 5 shows UV–vis spectra of the solution resulting from the PVA/PGLD-AgNPs systems after 24h. The presence of the SPR band in the PVA/PGLD hydrogels ensures the formation of AgNPs. The intensity of the absorbance obeys the Lambert-Beer law and is related to the concentration of the AgNPs in PVA/PGLD matrix[37]. Therefore, as observed in Figure 5, higher concentration of Cz-extract yields higher concentrations of AgNPs.

Figure 5 shows that the amount of Cz-extract also changes the wavelenght of absorbance band. The wavelenght of the SPR absorbance band is related to both, shape and the size of the AgNPs dispersed in the PVA/PGLD hydrogel[36]. The difference between the three reactional systems can be better observed upon normalizations of the absorbance band of the SPR, as shown in the inserted plot in Figure 5. The normalized absorbance curves show that the system with higher concentration of Cz-extract was more homogeneus and confirms the synergistic stabilizing and reduction properties of the *Cinnamomum verum* aqueous extract for the formation of AgNPs in the PVA/PGLD hydrogel matrix.

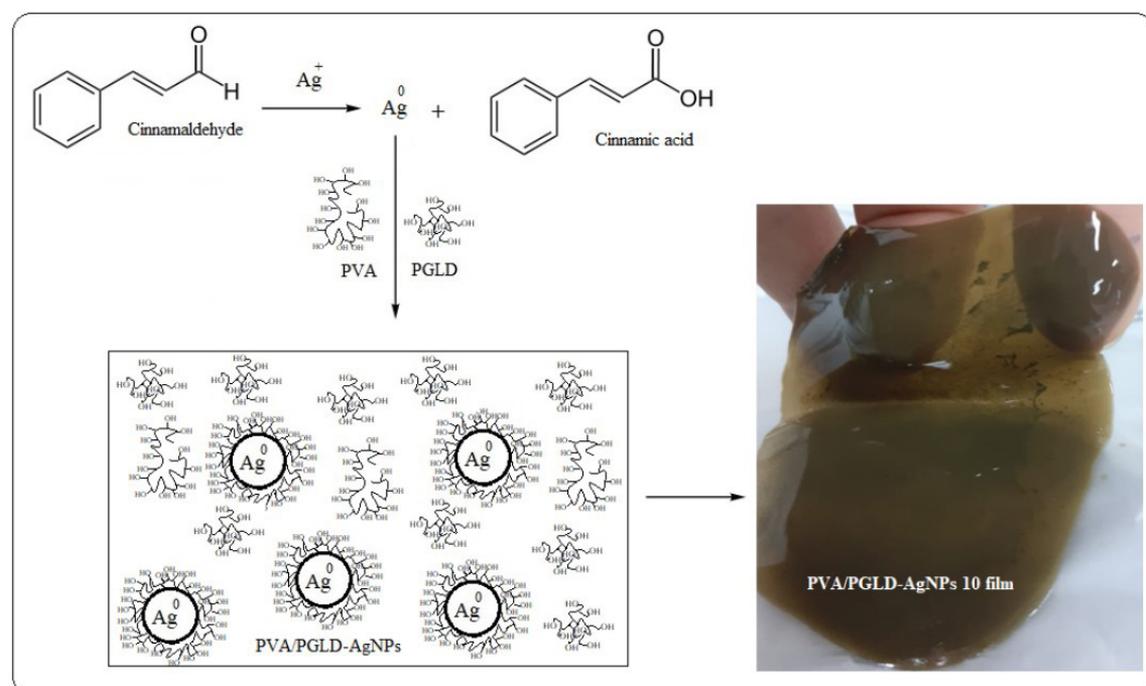FTIR spectroscopy was carried out on PVA/PGLD-AgNPs films to identify the organic funtional groups responsible

Figure 3. TGA/DTG of lyophilized Cz-extract.

Figure 4. Scheme of green synthesis from *Cinnamomum verum* aqueous extract. On the right is shown a photograph of the PVA/PGLD-AgNPs10 hydrogel after casting on PTFE plates.

for the stabilization of the AgNPs synthesized by Cz-extract and mediated by the PVA/PGLD hydrogel. Figure 6 shows the main stretching vibrations of chemical bonds in two wavenumber range (namely, 3600 – 2500 cm^{-1} and 1250 – 590 cm^{-1}). The -OH fuctional group is present in the Cz-extract as well as in the polymeric system. The films with 5 and 10 mL of Cz-extract shows O-H stretch vibrations at 3303 cm^{-1}. The film with higher Cz-extract amount showed O-H stretching vibration at 3273 cm^{-1}. This lower wavenumber suggests a decrease of the force constant of O-H bonds. This system has higher concentration of AgNPs and then requires more stabilization. Therefore, their results show that the -OH fuctional group of PVA and PGLD stabilizes the AgNPs being produced. According to the literature, the metal-OH interaction decreases the wavenumber of the O-H stretching vibrations[37].

The streching vibration at 2937 cm^{-1} is assigned to the -CH of alkane. The sharp absorptions at 1039 cm^{-1} corresponds to stretching vibration of C-O bonds. The vibration band observed at 675 cm^{-1} is assigned to bending vibration out of the plane of the O-H bond, associated with the peripheral hydroxyl groups (OH) on poly(glycerol) dendrimer.

Figure 7 shows the XRD pattern of the PVA/PGLD-AgNPs films at different concentrations of Cz-extract. The films show polycrystalline patterns with a broad reflection peaks at ~20° that was associated with PVA[38]. Diffraction peaks
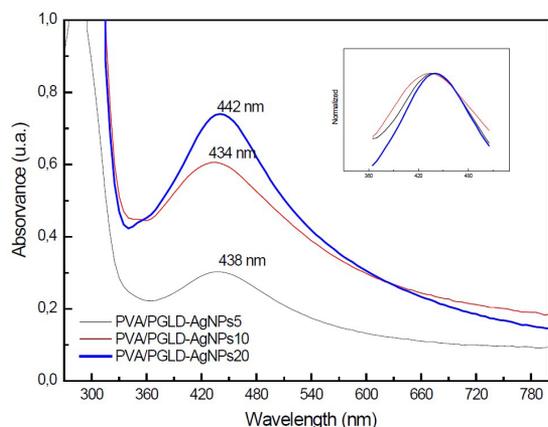
with values of 2θ near to 38.37°, 44.50°, 64.86°, 77.44° and 81.7° respectively corresponds to the XRD patterns indexed in [111], [200], [220], [311] and [222] lattice planes. These lattice planes is in good agreement with the metallic silver with face centered cubic structure[24,39]. The other observed crystalline peaks suggests the presence of organic crystaline substances in Cz-extract.

The average crystallite sizes of the AgNPs dispersed in the PVA/PGLD films was calculated using the Scherrer equation[18]:

$$D = \frac{k\lambda}{\beta \cos\theta} \qquad (3)$$

where D is the average crystallite size, k is the Scherrer constant, λ is the wavelength of the incident X-ray (for Cu Kα, λ = 0.154056 nm), while β and θ are the full width at half maximum of the intensity and the Bragg angle respectively.

Gaussian method was used to find the full width at half maximum (FWHM) in Origin software®. The average crystallite sizes calculated by Scherrer were 13.64 nm, 16.63nm and 20.27 nm for PVA-PGLD5, PVA-PGLD10 and film PVA-PGLD20, respectively. Relating the average crystallite sizes with the intensity of SPR absorbance bands observed in UV-Vis spectra, it can be concluded that the higher concentrations of AgNPs the higher the average crystallite size of AgNPs.

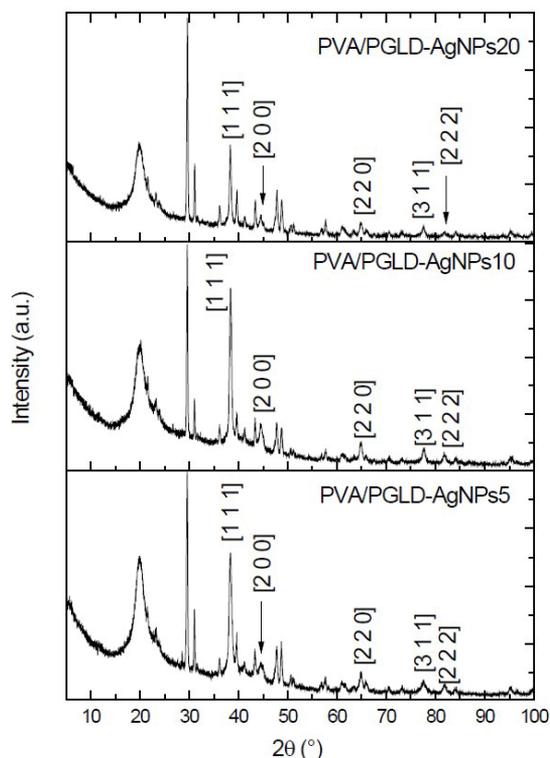The TGA-DTG analysis were carried out in order to evaluate the thermal stability and degradation profile of

Figure 5. UV–vis of green synthesis of the PVA/PGLD-AgNPs hydrogels.
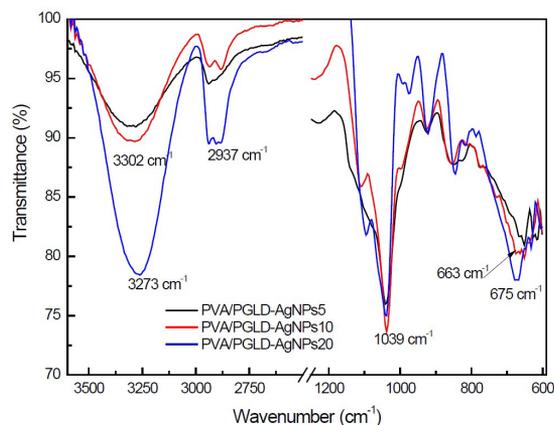
Figure 6. FTIR spectrum of PVA/PGLD-AgNPs films.

Figure 7. XRD spectra of the PVA/PGLDAgNPs films.

the PVA/PGLD-AgNPs hydrogels. The results are shown in Figure 8. The PVA/PGLD-AgNPs hydrogels shows two steps in its thermal degradation process (Fig. 8). The first step occurs between 25 ºC and 182 ºC, accompanied with the weight loss of 20%. This first degradation process could be assigned to the loss of adsorbed and the water physically bonded to hydrogels through hydrogen bonding, respectively. In turn, the weight loss around 180°C may be due to the loss of volatile organic substances present in Cz-extract. Following loss weight is observed between 180 ºC and 400 ºC approximately and it should correspond to the thermal decomposition of the PVA/PGLD matrix and can also be associated probably to the volatilization of the polyssacharides and carbohydrates from the Cz-extract. This thermal decomposition happed in one step suggesting a strong interaction between PVA, PGLD and Cz-extract. The observed solid residues can be ascribed to thermally stable compounds and AgNPs.

3.3 AgNPs release studies

Considering the theoretical studies[40], the estimated molar extinction coefficients from wavelength of the SPR band in Figure 4 were 839.82×10^8 $M^{-1}.cm^{-1}$, 773.36×10^8 $M^{-1}.cm^{-1}$ and 911.03×10^8 $M^{-1}.cm^{-1}$ for AgNPs synthesized using 5 mL, 10 mL and 20 mL of Cz-extract, respectively. These values were used to determine the concentration of AgNPs using the Lambert-Beer's law. The release of AgNPs from PVA/PGLD-AgNPs films were monitored along an interval of 24h at room temperature (25°C). The AgNPs release profiles measurements for each PVA/PGLD-AgNPs films are presented in Figure 9. It was observed a slow AgNPs release rates from PVA/PGLD-AgNPs (Figure 9). The AgNPs release from PVA/PGLD generally occurs by diffusion through the gelatinous layer or erosion of the hydrogel matrix or a combination of these mechanisms. Because AgNPs is poorly water soluble, their release from the PVA/PGLD matrix system is likely to be predominately controlled by the dissolution rate of the hydrogel. The amount of Cz-extract incorporated in the PVA/PGLD seems to have a significant effect on the formation of the PVA/PGLD hydrogel matrix (Figure 9). The PGLD/PVA formulation with higher amounts of Cz-extract seems to create PGLD/PVA hydrogels matrices with lower crosslinking density relative to formulations with smaller amounts of the extract (PVA/PGLD-AgNPs5). Interestingly, AgNPs released from the PGLD/PVA-AgNP20 exibited an anomalous behavior and showed a relatively slow release realively to PVA/PGLD-AgNPs5 and PVA/PGLD-AgNPs10 matrices. Perhaps there is some critical concentration of Cz-extract for the formation of PVA/PGLD hydrogels with high crosslinking density and that promote a slower erosion rate and thus a slower AgNPs release rate. However, further research is needed

to investigate the critical Cz-extract concentration to form mechanically more stable PVA/PGLD hydrogels matrices.

The obtained kinetic rate constant K, the correlation coefficient R^2 and the release exponents n are given in Table 1.

The AgNPs releases from PVA/PGLD-AgNPs films were best fitted by Korsmeyer–Peppas model (Table 1). This model is used to describe the diffusion of a penetrant solute in a swellable polymeric matrix. Therefore, Korsmeyer–Peppas model can be applied to a hydrogel polymer that sorbs the solvent and desorbs the loaded active principle.

In the Korsmeyer–Peppas model, the exponent "n" is related to release mechanism of active principle. For a single thin film with $0.5 < n < 1$, the system can be described as an anomalous transport (non-Fickian diffusion)[29]. For PVA/PGLD-AgNPs5 and PVA/PGLD-AgNPs20 films, the values of the exponent "n" were larger than 0.5 and smaller than 1, indicating that a non-Fickian diffusion mechanism was dominant for the release of AgNPs. The mechanism
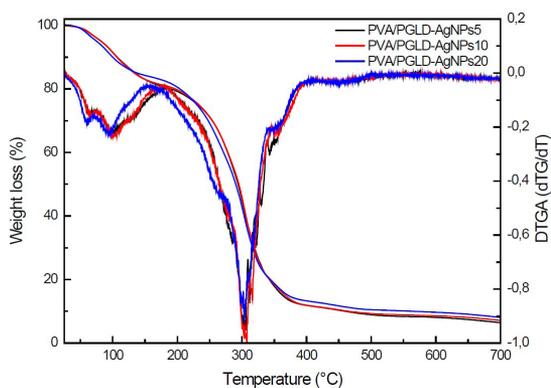

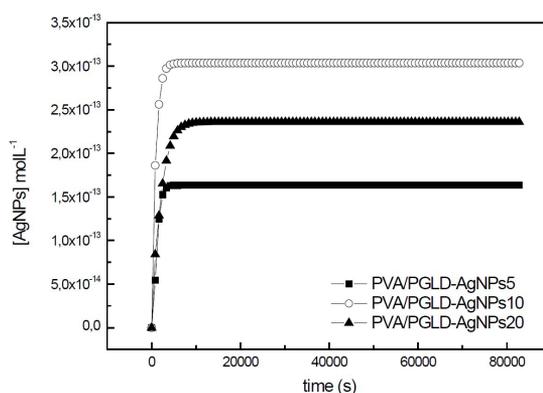**Figure 8.** TGA/DTG of the PVA/PGLD-AgNPs films.

Figure 9. AgNPs release profile of the PVA/PGLD-AgNPs films.

Table 1. Release kinetics of silver nanoparticles.

Films	Higuchi		Korsmeyer-Peppa		
	k_H	R^2	n	k_{KP}	R^2
PVA/PGLD AgNPs5	8.71×10^{-17}	0.93	0.96	5.33×10^{-4}	0.95
PVA/PGLD AgNPs10	1.28×10^{-14}	0.91	0.39	4.23×10^{-2}	0.97
PVA/PGLD AgNPs20	1.33×10^{-15}	0.98	0.61	5.60×10^{-3}	1.00

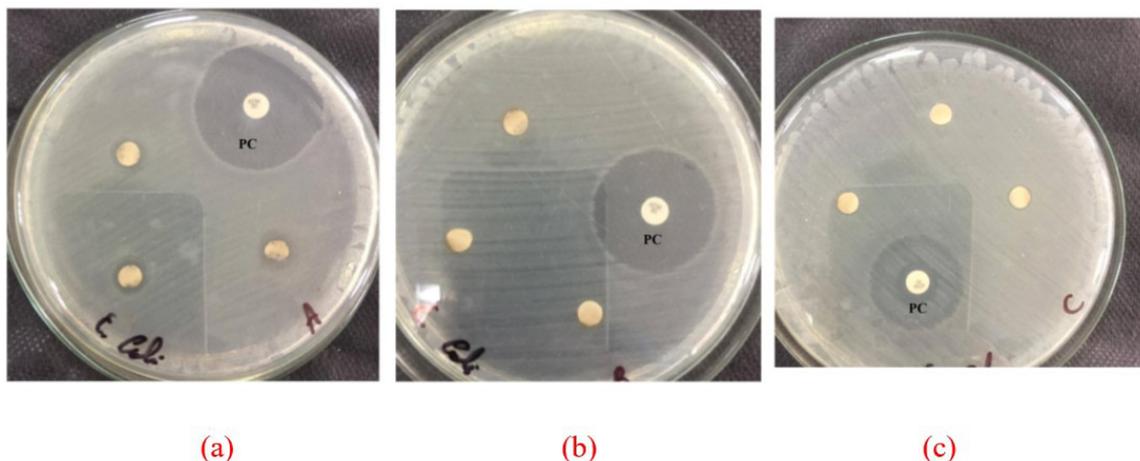(a)   (b)   (c)

Figure 10. Antimicrobial activities of AgNPs against *E. coli* (a) PVA/PGLD-AgNPs5; (b) PVA/PGLD-AgNPs10; (c) PVA/PGLD-AgNPs20 (PC positive control).

of release from PVA/PGLD10 film shows n < 0.5 values. Therefore, this system can be mechanistically identified as a quasi-Fickian diffusion. The Korsmeyer–Peppas kinetic rate constant, K_{KP}, was higher in the PVA/PGLD10 film, suggesting a faster AgNPs release in this Cz-extract composition. These results reveals that the PVA/PGLD network changes with the amount of Cz-extract used in the green synthesis of the AgNPs.

3.4 Antimicrobial properties

The antimicrobial activities of the PVA/PGLD-AgNPs were investigated by disk diffusion method. Figure 10 shows the inhibition zone against *E. coli* for all films.

Comparison of these results indicates that, for *E.coli*, the PVA/PGLD-AgNPs5 film presents a higher inhibition zone (7.93±0.05 mm) than the PVA/PGLD-AgNPs10 and PVA/PGLD-AgNPs20 films (6.05±0.03 mm). This may be attributed to the different size and concentrations of AgNPs released from PVA/PGLD hydrogel matrices. The PVA/PGLD-AgNPs5 film releases the lowest concentration of AgNPs, however its nanoparticles are smaller in size which could contribute to greater efficiency against *E. coli* bacteria.

4. Conclusions

Silver nanoparticles were successfully obtained by green synthesis using *Cinnamomum verum* aqueous extract, mediated by poly(vinyl alcohol)/poly(glycerol) dendrimer hydrogel. The UV-Vis, FTIR and TGA techniques of characterization showed that the extract of *Cinnamomum verum* bark contains phytochemical compounds with reducing properties and capping agent to stabilize AgNPs. The SPR band in the UV-vis spectra confirmed the formation of AgNPs. XRD pattern confirmed the presence of metallic silver with crystalline structure of face centered cubic. It was observed that the average crystallite size calculated by Scherrer equation was related with the amount of Cz-extract used, and to the concentration of AgNPs in the PVA/PGLD matrix. The residues obtained by TGA analysis confirmed

that the concentration of AgNPs is related with the amount of Cz-extract used in the green synthesis. The in vitro study of AgNPs release showed that all PVA/PGLD-AgNPs films are capable of controlling AgNPs release from the hydrogels and were best fitted by Korsmeyer–Peppas model. All PVA/PGLD-AgNPs films showed antibacterial properties against *E. coli* which are related to the size of AgNPs.

5. Author's Contribution

- **Conceptualization** – Maria Elena Leyva González; Gisela Helou Rosas; Alvaro Antonio Alencar de Queiroz.
- **Data curation** – Pollyana Marcondes; Paulo Sergio Marques.
- **Formal analysis** – Maria Elena Leyva González.
- **Funding acquisition** – Maria Elena Leyva González.
- **Investigation** – Pollyanna Marcondes; Paulo Sergio Marques.
- **Methodology** – Maria Elena Leyva González.
- **Project administration** – Maria Elena Leyva González.
- **Resources** – Alvaro Antonio Alencar de Queiroz.
- **Software** – NA.
- **Supervision** – Maria Elena Leyva González; Gisela Helou Rosas.
- **Validation** – Maria Elena Leyva González; Gisela Helou Rosas; Alvaro Antonio Alencar de Queiroz.
- **Visualization** – Maria Elena Leyva González; Alvaro Antonio Alencar de Queiroz.
- **Writing – original draft** – Maria Elena Leyva González.
- **Writing – review & editing** – Maria Elena Leyva González; Alvaro Antonio Alencar de Queiroz.

6. Acknowledgements

7. References

1. Forjuoh, S. N. (2006). Burns in low- and middle-income countries: a review of available literature on descriptive epidemiology, risk factors, treatment, and prevention. *Burns*, *32*(5), 529-537. http://dx.doi.org/10.1016/j.burns.2006.04.002. PMid:16777340.

2. Aghakhani, N., Nia, H. S., Soleimani, M. A., Bahrami, N., Rahbar, N., Fattahi, Y., & Beheshti, Z. (2011). Prevalence burn injuries and risk factors in persons older the 15 years in Urmia burn center in Iran. *Caspian Journal of Internal Medicine*, *2*(2), 240-244. PMid:24024024.

3. Abib, S. C. V., Françóia, A. M., Waksman, R., Dolci, M. I., Guimarães, H. P., Moreira, F., Cezillo, M. V. B., & Góes, A. M., Jr. (2017). Unintentional pediatric injuries in São Paulo. How often is it severe? *Acta Cirurgica Brasileira*, *32*(7), 587-598. http://dx.doi.org/10.1590/s0102-865020170070000010. PMid:28793043.

4. Hohl, D. H., Coltro, P. S., Silva, G. M. A., Silveira, V. G., & Farina, J. A., Jr. (2021). Covid-19 quarantine has increased the incidence of ethyl alcohol burns. *Burns*, *47*(5), 1212. http://dx.doi.org/10.1016/j.burns.2020.05.025. PMid:34034953.

5. Valente, T. M., Ferreira, L. P. S., Silva, R. A., Leite, J. M. R. S., Tiraboschi, F. A., & Barboza, M. C. C. (2021). Brazil Covid-19: change of hospitalizations and deaths due to burn injury? *Burns*, *47*(2), 479-501. http://dx.doi.org/10.1016/j.burns.2020.10.009. PMid:33303263.

6. Barillo, D. J., & Marx, D. E. (2014). Silver in medicine: a brief history BC 335 to present. *Burns*, *40*(Suppl. 1), S3-S8. http://dx.doi.org/10.1016/j.burns.2014.09.009. PMid:25418435.

7. Klasen, H. J. (2000). Historical review of the use of silver in the treatment of burns. I. Early uses. *Burns*, *26*(2), 117-130. http://dx.doi.org/10.1016/S0305-4179(99)00108-4. PMid:10716354.

8. Klasen, H. J. (2000). A historical review of the use of silver in the treatment of burns. II. Renewed interest for silver. *Burns*, *26*(2), 131-138. http://dx.doi.org/10.1016/S0305-4179(99)00116-3. PMid:10716355.

9. Atiyeh, B. S., Costagliola, M., Hayek, S. N., & Dibo, S. A. (2007). Effect of silver on burn wound infection control and healing: review of the literature. *Burns*, *33*(2), 139-148. http://dx.doi.org/10.1016/j.burns.2006.06.010. PMid:17137719.

10. Walker, M., & Parsons, D. (2014). The biological fate of silver ions following the use of silver-containing wound care products – a review. *International Wound Journal*, *11*(5), 496-504. http://dx.doi.org/10.1111/j.1742-481X.2012.01115.x. PMid:23173975.

11. Shaheen, H. M. (2016). Wound healing and silver nanoparticles. *Global Drugs Therapeutics*, *1*(1), 1-2. http://dx.doi.org/10.15761/GDT.1000105. PMid:27534756.

12. Zhang, K., Lui, V. C. H., Chen, Y., Lok, C. N., & Wong, K. K. Y. (2020). Delayed application of silver nanoparticles reveals the role of early infammation in burn wound healing. *Scientific Reports*, *10*(1), 6338. http://dx.doi.org/10.1038/s41598-020-63464-z. PMid:32286492.

13. Lee, B., Lee, M. J., Yun, S. J., Kim, K., Choi, I., & Park, S. (2019). Silver nanoparticles induce reactive oxygen species-mediated cell cycle delay and synergistic cytotoxicity with 3-bromopyruvate in Candida albicans, but not in Saccharomyces cerevisiae. *International Journal of Nanomedicine*, *14*, 4801-4816. http://dx.doi.org/10.2147/IJN.S205736. PMid:31308659.

14. Reidy, B., Haase, A., Luch, A., Dawson, K. A., & Lynch, I. (2013). Mechanisms of silver nanoparticle release, transformation and toxicity: a critical review of current knowledge and recommendations for future studies and applications. *Materials (Basel)*, *6*(6), 2295-2350. http://dx.doi.org/10.3390/ma6062295. PMid:28809275.

15. Habibullah, G., Viktorova, J., & Ruml, T. (2021). Current strategies for noble metal nanoparticle synthesis. *Nanoscale Research Letters*, *16*(1), 47. http://dx.doi.org/10.1186/s11671-021-03480-8. PMid:33721118.

16. Jha, A. K., Prasad, K., Prasad, K., & Kulkarni, A. R. (2009). Plant system: nature's nanofactory. *Colloids and Surfaces. B, Biointerfaces*, *73*(2), 219-223. http://dx.doi.org/10.1016/j.colsurfb.2009.05.018. PMid:19539452.

17. Santhoshkumar, J., Rajeshkumar, S., & Venkat Kumar, S. (2017). Phyto-assisted synthesis, characterization and applications of gold nanoparticles: a review. *Biochemistry and Biophysics Reports*, *11*, 46-57. http://dx.doi.org/10.1016/j.bbrep.2017.06.004. PMid:28955767.

18. Alwan, S. H., & Al-Saeed, M. H. (2021). Biosynthesized silver nanoparticles (using *Cinnamomum verum* bark extract) improve the fertility status of rats with polycystic ovarian syndrome. *Biocatalysis and Agricultural Biotechnology*, *38*, 102217. http://dx.doi.org/10.1016/j.bcab.2021.102217.

19. Kumar, S., Kumari, R., & Mishra, S. (2019). Pharmacological properties and their medicinal uses of Cinnamomum: a review. *The Journal of Pharmacy and Pharmacology*, *71*(12), 1735-1761. http://dx.doi.org/10.1111/jphp.13173. PMid:31646653.

20. Ghosh, T., Basu, A., Adhikari, D., Roy, D., & Pal, A. K. (2015). Antioxidant activity and structural features of Cinnamomum zeylanicum. *3 Biotech*, *5*(6), 939-947. PMid:28324396.

21. Maruthamuthu, R., & Ramanathan, K. (2016). Phytochemical analysis of bark extract of cinnamomum verum: a medicinal herb used for the treatment of coronary heart disease in malayali tribes, Pachamalai Hills, Tamil Nadu, India. *International Journal of Pharmacognosy and Phytochemical Research*, *8*(7), 1218-1222. Retrieved in 2022, November 23, from https://www.researchgate.net/publication/305326819

22. Doyle, A. A., & Stephens, J. C. (2019). A review of cinnamaldehyde and its derivatives as antibacterial agents. *Fitoterapia*, *139*, 104405. http://dx.doi.org/10.1016/j.fitote.2019.104405. PMid:31707126.

23. Saki, M., Seyed-Mohammadi, S., Montazeri, E. A., Siahpoosh, A., Moosavian, M., & Latifi, S. M. (2020). In vitro antibacterial properties of Cinnamomum verum essential oil against clinical extensively drug-resistant bacteria. *European Journal of Integrative Medicine*, *37*, 101146. http://dx.doi.org/10.1016/j.eujim.2020.101146.

24. Sathishkumar, M., Sneha, K., Won, S. W., Cho, C., Kim, S., & Yun, Y. (2009). Cinnamon zeylanicum bark extract and powder mediated green synthesis of nano-crystalline silver particles and its bactericidal activity. *Colloids and Surfaces. B, Biointerfaces*, *73*(2), 332-338. http://dx.doi.org/10.1016/j.colsurfb.2009.06.005. PMid:19576733.

25. Smitha, S. L., Philip, D., & Gopchandran, K. G. (2009). Green synthesis of gold nanoparticles using Cinnamomum zeylanicum leaf broth. *Spectrochimica Acta. Part A: Molecular and Biomolecular Spectroscopy*, *74*(3), 735-739. http://dx.doi.org/10.1016/j.saa.2009.08.007. PMid:19744880.

26. Ansari, M. A., Murali, M., Prasad, D., Alzohairy, M. A., Almatroudi, A., Alomary, M. N., Udayashankar, A. C., Singh, S. B., Asiri, S. M. M., Ashwini, B. S., Gowtham, H. G., Kalegowda, N., Amruthesh, K. N., Lakshmeesha, T. R., & Niranjana, S. R. (2020). Cinnamomum verum bark extract mediated green synthesis of ZnO nanoparticles and their antibacterial potentiality. *Biomolecules*, *10*(2), 336. http://dx.doi.org/10.3390/biom10020336. PMid:32092985.

27. Liu, H., Wang, G., Liu, J., Nan, K., Zhang, J., Guo, L., & Liu, Y. (2021). Green synthesis of copper nanoparticles using Cinnamomum zelanicum extract and its applications as a highly efficient antioxidant and anti-human lung carcinoma. *Journal of Experimental Nanoscience*, *16*(1), 410-423. http://dx.doi.org/10.1080/17458080.2021.1991577.

28. Oliveira, M. L. P., Wanderley Neto, E. T., Queiroz, A. A. A. E., & Queiroz, A. A. A. (2021). Intelligent optical temperature sensor based on polyglycerol dendrimer microspheres encapsulating hopeites. *Materials Research*, *24*(4), e20200568. http://dx.doi.org/10.1590/1980-5373-mr-2020-0568.

29. Siepmann, J., & Siepmann, F. (2008). Mathematical modeling of drug delivery. *International Journal of Pharmaceutics*, *364*(2), 328-343. http://dx.doi.org/10.1016/j.ijpharm.2008.09.004. PMid:18822362.

30. Siepmann, J., & Peppas, N. A. (2011). Higuchi equation: derivation, applications, use and misuse. *International Journal of Pharmaceutics*, *418*(1), 6-12. http://dx.doi.org/10.1016/j.ijpharm.2011.03.051. PMid:21458553.

31. Balouiri, M., Sadiki, M., & Ibnsouda, S. K. (2016). Methods for in vitro evaluating antimicrobial activity: A review. *Journal of Pharmaceutical Analysis*, *6*(2), 71-79. http://dx.doi.org/10.1016/j.jpha.2015.11.005. PMid:29403965.

32. Rind, F. M. A., Memon, A. H., Almani, F., Laghari, M. G. H., Mughal, U. R., Maheshwari, M. L., & Khuhawar, M. Y. (2011). Spectrophotometric determination of Cinnamaldehyde from crude drugs and herbal preparations. *Asian Journal of Chemistry*, *23*(2), 631-635. Retrieved in 2022, November 23, from https://asianjournalofchemistry.co.in/user/journal/viewarticle.aspx?ArticleID=23_2_38

33. Singh, G., Maurya, S., deLampasona, M. P., & Catalan, C. A. N. (2007). A comparison of chemical, antioxidant and antimicrobial studies of cinnamon leaf and bark volatile oils, oleoresins and their constituents. *Food and Chemical Toxicology*, *45*(9), 1650-1661. http://dx.doi.org/10.1016/j.fct.2007.02.031. PMid:17408833.

34. Silva, A. M. R., Ferreira, N. L. O., Oliveira, A. E., Borges, L. L., & Conceição, E. C. (2017). Comparison of ultrasound-assisted extraction and dynamic maceration over content of tagitinin C obtained from Tithonia diversifolia (Hemsl.) A. gray leaves using factorial design. *Pharmacognosy Magazine*, *13*(50), 270-274. http://dx.doi.org/10.4103/0973-1296.204555. PMid:28539720.

35. Bach, Q., & Chen, W. (2017). Pyrolysis characteristics and kinetics of microalgae via thermogravimetric analysis (TGA): A state-of-the-art review. *Bioresource Technology*, *246*, 88-100. http://dx.doi.org/10.1016/j.biortech.2017.06.087. PMid:28709883.

36. Wu, C., Zhou, X., & Wei, J. (2015). Localized surface plasmon resonance of silver nanotriangles synthesized by a versatile solution reaction. *Nanoscale Research Letters*, *10*(1), 354. http://dx.doi.org/10.1186/s11671-015-1058-1. PMid:26340946.

37. Salazar-Salinas, K., Baldera-Aguayo, P. A., Encomendero-Risco, J. J., Orihuela, M., Sheen, P., Seminario, J. M., & Zimic, M. (2014). Metal-ion effects on the polarization of metal-bound water and infrared vibrational modes of the coordinated metal center of mycobacterium tuberculosis pyrazinamidase via quantum mechanical calculations. *The Journal of Physical Chemistry B*, *118*(34), 10065-10075. http://dx.doi.org/10.1021/jp504096d. PMid:25055049.

38. Ricciardi, R., Auriemma, F., De Rosa, C., & Lauprêtre, F. (2004). X-ray diffraction analysis of Poly(vinyl alcohol) hydrogels obtained by freezing and thawing techniques. *Macromolecules*, *37*(5), 1921-1927. http://dx.doi.org/10.1021/ma035663q.

39. Liu, C., Yang, X., Yuan, H., Zhou, Z., & Xiao, D. (2007). Preparation of silver nanoparticle and its application to the determination of ct-DNA. *Sensors (Basel)*, *7*(5), 708-718. http://dx.doi.org/10.3390/s7050708.

40. Paramelle, D., Sadovoy, A., Gorelik, S., Free, P., Hobley, J., & Fernig, D. G. (2014). Rapid method to estimate the concentration of citrate capped silver nanoparticles from UV-visible light spectra. *The Analyst*, *139*(19), 4855-4861. http://dx.doi.org/10.1039/C4AN00978A. PMid:25096538.